Articles in PresS. Am J Physiol Lung Cell Mol Physiol (March 23, 2017). doi:10.1152/ajplung.00554.2016

The Innate Immune Response in Fetal Lung Mesenchymal Cells Targets VEGFR2 Expression and Activity

Rachel M. Medal[a], Amanda M. Im[b], Yasutoshi Yamamoto[b], Omar Lakhdari[a], Timothy S. Blackwell[b], Hal M. Hoffman[a], Debashis Sahoo[a], and Lawrence S. Prince[a]#

Department of Pediatrics, University of California, San Diego and Rady Children's Hospital, San Diego, California, USA[a]; Departments of Pediatrics, Medicine, Developmental and Cell Biology, and Cancer Biology, Vanderbilt University School of Medicine, Nashville, Tennessee, USA[b].

Running Title: Innate Immune Response in Lung Mesenchymal Cells

#Address Correspondence to:

Lawrence Prince
Associate Professor of Pediatrics
Division Chief of Neonatology
Rady Children's Hospital, San Diego
University of California, San Diego
4115 Biomedical Research Facility 2
Mail Code 0760
9500 Gilman Drive
La Jolla, CA 92093-0760
(858)-822-4677
lprinceucsd@gmail.com

ABSTRACT

In preterm infants, soluble inflammatory mediators target lung mesenchymal cells, disrupting airway and alveolar morphogenesis. However, how mesenchymal cells respond directly to microbial stimuli remains poorly characterized. Our objective was to measure the genome-wide innate immune response in fetal lung mesenchymal cells exposed to the bacterial endotoxin lipopolysaccharide (LPS). Using Affymetrix MoGene 1.0st arrays, we showed that LPS induced expression of unique innate immune transcripts heavily weighted toward CC and CXC family chemokines. The transcriptional response was different between cells from E11, E15, and E18 mouse lungs. In all cells tested, LPS inhibited expression of a small core group of genes including the VEGF receptor *Vegfr2*. While best characterized in vascular endothelial populations, we demonstrated here that fetal mouse lung mesenchymal cells express *Vegfr2* and respond to VEGF-A stimulation. In mesenchymal cells, VEGF-A increased cell migration, activated the ERK/AKT pathway, and promoted FOXO3A nuclear exclusion. Using an experimental co-culture model of epithelial-mesenchymal interactions, we also showed that VEGFR2 inhibition prevented formation of 3-dimensional structures. Both LPS and tyrosine kinase inhibition reduced 3-dimensional structure formation. Our data suggest a novel mechanism for inflammation-mediated defects in lung development involving reduced VEGF signaling in lung mesenchyme.

INTRODUCTION

Lung mesenchymal cells play key roles in development and repair. During airway branching morphogenesis, mesenchymal growth factors signal adjacent airway epithelia and stimulate airway elongation and expansion (27, 47, 58). Coordinated paracrine feedback mechanisms regulate the temporal and spatial dynamics during lung branching. Fetal lung mesenchyme also guides formation of the pulmonary circulation (64). In addition to their roles in lung morphogenesis, fetal lung mesenchymal cells have multipotent properties. Similar to mesenchymal stem cells or stromal cells in other fetal and adult tissues, lung mesenchymal cells can differentiate into multiple cell types, including vascular endothelium, smooth muscle, cartilage, and a diverse set of fibroblast populations (3, 18, 34, 36, 39, 40, 46, 66). While lung branching morphogenesis completes during fetal life, ongoing mesenchymal cell differentiation, vascular development, and alveolar formation occur well after birth (17, 49).

Lung mesenchymal cells also play a central role in regulating inflammation, preventing injury, and mediating repair. In many of the most preterm patients, injury and inflammation causes abnormal lung development, giving rise to the chronic developmental disease termed bronchopulmonary dysplasia (BPD, (65)). BPD pathogenesis likely involves failure of appropriate development and repair following injury (4, 32). Among the many exposures thought to play a role in BPD pathogenesis, infection and inflammation appear to be the major environmental factors that inhibit normal development and cause disease (42). In the lung, macrophages and airway epithelial cells are the first responders to inhaled pathogens. Mesenchymal cells then

appear to regulate the inflammatory response and mediate repair. While many reports have described the anti-inflammatory and trophic functions of lung mesenchymal cells and mesenchymal stromal cells, how these mesenchymal cell populations respond to microbial signals remains unclear. Given their role in lung morphogenesis and repair, better understanding of how lung mesenchymal cells, and particularly cells from the developing lung, respond to innate immune stimuli is key to developing new strategies aimed at reducing lung injury and facilitating normal recovery.

Studying the unique biological behaviors of lung mesenchymal cells is complicated by standard cell culture techniques. When passaged for multiple generations, cultures of lung mesenchymal cells begin to resemble more homogeneous lung fibroblast cell lines. To overcome this potential loss of biological complexity, we previously isolated and characterized fetal mouse lung mesenchymal cell lines from transgenic $SV40^{tsA58}$ mice (Immortomice (33)). Mesenchymal cell lines from these mice universally expressed α-smooth muscle actin (SMA) under standard culture conditions but displayed multipotent properties when cultured with specific growth factors (33). Interestingly, these lung mesenchymal cells expressed basal levels of *Vegfr2* mRNA and low levels of VEGFR2 protein. Treating cells with VEGF and FGF-2 increased VEGFR2 protein expression to more detectable levels and promoted endothelial differentiation.

Here we use these cells to test the fetal lung mesenchymal transcriptional response to the TLR4 agonist lipopolysaccharide (LPS) to better understand how inflammation might affect global gene expression. Using conditionally immortalized cell lines allowed us to

maintain cell viability and heterogeneity during expansion. Using cells isolated from different stages of lung development also provided a broader assessment of how these cells respond to innate immune stimuli. Interestingly, LPS inhibited mesenchymal *Vegfr2* expression and disrupted the mesenchymal response to VEGF. These data shed new insight into how inflammation alters mesenchymal gene expression and therefore potentially influences cell biology.

MATERIALS AND METHODS

Animal studies, cell culture, and reagents

All animal procedures were performed with approval of the Institutional Animal Care and Use Committees at the University of California San Diego and Vanderbilt University. Fetal lung mesenchymal cell lines isolated from E11, E15, and E18 Immortomice (Charles River) expressing the temperature sensitive early region SV40 mutant tsA58 allele were maintained at 33˚C in DMEM with 10% FBS with penicillin/streptomycin supplemented with IFN-γ. All cells were moved to 37 ˚C and passaged at least once before plating for RNA isolation. Cells were seeded at equal density on 6 separate 100 mm dishes. Once the cells reached 80-90% confluency, they were switched to serum-free DMEM for 4 h. 3 plates were then treated with 250 ng/ml *E. coli* LPS (strain O55:B5, Sigma, L6529). The other 3 plates remained in serum free DMEM. At 4 h, 24 h, and 48 h after treatment, a pair of plates (1 control and 1 LPS-treated) was harvested using TRIzol (Thermo Fisher). RNA was isolated using standard techniques and DNAse treatment. For replicates, serial passages of each cell line were used. The entire experiment was conducted three separate times for each condition and time point, generating 54 RNA samples for microarray analysis. For gene silencing experiments, cells were transfected with pre-designed siRNAs targeting *Vegfr1*, *Vegfr2,* or luciferase using the Nter system (Sigma)(25). Wound closure assays were performed 48 hours following transfection.

E15 primary lung mesenchymal cells from C57BL/6 mice (Harlan) were isolated from minced lung tissue via outgrowth onto plastic dishes in DMEM with 10% FBS and

penicillin/streptomycin(5-7, 21). When the cells grew to confluence, the lung tissue was removed under a dissecting microscope, leaving mesenchymal cells behind. Cells were then passaged once prior to using in experiments. A549 human epithelial cells were obtained from ATCC and cultured in DMEM with 10% FBS and penicillin/streptomycin. For co-culture experiments, primary fetal lung mesenchymal cells were plated at high density (3.125×10^5 cells/cm^2) and grown to confluence. A549 cells were then overlaid at similar cell density to encourage complete coverage of the underlying mesenchyme. Following overnight attachment, non-adherent cells were washed extensively. Co-cultures were then maintained in DMEM with 10% FBS for 3 d prior to analysis. Peak number was quantified by counting discrete, visible 3-dimensional peaks by dark-field microscopy. To measure peak height, co-cultures were first immunostained using antibodies against α-smooth muscle actin and E-cadherin. 3-dimensional laser scanning confocal microscopy was used to measure the height of discrete peaks.

Antibodies

Cy3-labeled mouse anti-alpha smooth muscle actin (C6198) was purchased from Sigma. AZD2171 (S1017) and MGCD265 (S1361) were purchased from Selleckchem. Rabbit anti-Vegfr2 (2479), rabbit anti-phospho-Vegfr2 (4991), rabbit anti-phospho-Erk1/2 (4277), rabbit anti Akt (4685), rabbit anti-phospho-Akt (2965), rabbit anti-Erk1 (4372), rabbit anti-Erk2 (9108), and rabbit anti FOXO3A (12829) were purchased from Cell Signaling Technology. Rat anti-E-cadherin (ECCD-2), peroxidase-conjugated goat anti-rabbit and Alexa488-conjugated goat anti-rabbit antibodies were purchased from Thermo-Fisher.

RNA isolation, microarray hybridization, and real-time PCR

Total RNA was isolated using TRIzol Reagent and quantified by spectroscopy; RNA quality was determined using a Bioanalyzer 2100 (Aglient Technologies). Samples with high RIN scores (> 7) were prepared for microarray analysis using standard Affymetrix protocols in the Vanderbilt Technologies for Advanced Genomics Shared Resource. Samples were hybridized to Affymetrix Mouse Gene 1.0 ST arrays, washed, stained, and scanned using a GeneTitan Multichannel Instrument.

cDNA for real-time PCR was generated using a modified MMLV reverse transcriptase (SuperScript III; Life Technologies, 18080-051) and oligo dT primers. Gene specific TaqMan primer sets (Life Technologies) were used to quantitate *Gapdh*, *Ccl2*, *Vegfr1*, and *Vegfr2* in biological triplicates as well as technical triplicates, reactions were run using with IQ Supermix (Bio-Rad, 170-8862) on a CFX96 Touch system (Bio-Rad). Expression of each gene was compared with *Gapdh* and expressed as a fold change using the $2^{-\Delta\Delta C}{}_T$ method (41). Differences in expression between groups were compared by one-way ANOVA, all values were presented as the mean + SEM.

Microarray analysis

Affymetrix CEL images were imported directly into Bioconductor (version 3.0) within R (version 3.1.1, http://www.r-project.org). All the datasets were preprocessed and background corrected using the MAS method, constant normalization, PM-only probe specific correction and expression summarized using the Li Wong method. Differential

gene expression analysis was performed using a linear model and empirical Bayes methods within the *limma* package (54, 61). Translation from gene list of differentially expressed genes to gene ontologies (GO) was performed using the functional annotation tool in DAVID (30, 31). Visualization of summarized GO terms was performed using the web server REVIGO's treemap analysis (62). Unsupervised hierarchical clustering was performed using ArrayStudio (OmicSoft) complete linkage analysis to determine euclidean distance.

Boolean gene correlation

For Boolean gene correlation, the web based BooleanNet was used to query publically available microarray data sets using the Human U133 Plus 2.0 platform. *VEGFR2* expression was queried and compared to expression of *CDH5* and *PECAM1*. Samples including "mesenchyme" or "mesenchymal" in their descriptions were highlighted.

Wound closure assay

E15 mesenchymal cells from Immortomice were passaged once at 37˚C before being plated at 80% confluence. Cells were recovered overnight, serum starved for 6 hours, and pretreated with LPS. Wounds were then inflicted to the monolayer using a P200 pipet tip drawn down the center of the well. Nonadherent cells were then gently washed away with PBS. Serum free media containing heparin alone (50 μg/ml), recombinant VEGF-A with heparin (10 ng/mL), or recombinant PDGF-BB with heparin (20 ng/mL) was then added. Images were obtained immediately after wounding and then following 30 hours of

206 culture. Percentage of wound area that was covered by cells at 30 h was measured using
207 ImageJ (NIH) and the MRI Wound Healing Tool.
208
209 ***Western blotting***
210 Cell lysates were prepared as described previously and separated by SDS/PAGE (66).
211 Membranes were blocked in 5% milk in TRIS-buffered saline containing 0.05% Tween-
212 20 (TBST). Primary antibodies (1:1000 in TBST) were incubated with blocked
213 membranes overnight at 4˚C and developed by enhanced chemiluminescence using
214 peroxidase-conjugated secondary antibodies.
215
216 *Immunostaining*
217 Cells were cultured on coverslips, fixed, permeabilized, blocked, and then labeled with
218 anti-FOXO3A antibodies. Staining was visualized using an Alexa488-conjugated
219 secondary antibody. Nuclei were labeled with Draq5. Cells were then imaged using a
220 Leica SPE inverted laser scanning confocal microscope. To measure nuclear FOXO3A
221 localization, mean pixel intensity in the 488 nm channel was quantified within Draq5
222 labeled nuclear structures. 29 different cells were measured for each condition.
223
224

RESULTS

Inflammatory mediators target fetal lung mesenchymal cells, disrupt developmental gene expression, and inhibit airway morphogenesis (5-7, 52). However, how mesenchymal cells directly respond to innate immune stimuli at the molecular and genomic levels remains unclear. Figure 1A,B demonstrates that LPS-treated fetal lung mesenchymal cells are more elongated and spindle-shaped, suggesting LPS can at least induce morphological changes in lung mesenchymal cells. To measure the lung mesenchymal innate immune response and test how it might change during development, we treated fetal lung mesenchymal cell lines from E11, E15, and E18 *SV40*^{tsA58} mice with LPS for 4 h, 24 h, and 48 h. RNA from control and LPS-treated cells was profiled using Affymetrix Mouse Gene 1.0 ST microarrays. Principal component analysis (PCA) demonstrated that transcriptional profiles clustered based on developmental time point from which the cell lines were isolated (Figure 1C). To identify differentially expressed genes, we used the *limma* linear model approach (54, 61) that uses a Bayesian framework to compare gene-wise variances across large datasets ($p < 0.01$). An independent unsupervised hierarchical clustering analysis was performed on all samples clustering both arrays and genes (Figure 1D). LPS increased the expression of more genes than were repressed. Across all time points, 775 genes were differentially expressed following LPS treatment, with 490 genes increased and 285 decreased (Figure 1E) (55).

We next focused on the early innate immune response in lung mesenchymal cells by analyzing changes in gene expression following 4 h of LPS treatment. Unsupervised hierarchical clustering demonstrated that most of the 4 h LPS response involved

248 increased gene expression with a smaller number of down regulated genes (Figure 2A).
249 Samples were then further clustered by the embryonic stage from which the cell lines
250 were isolated. The changes in gene expression following 4 h of LPS treatment were
251 relatively unique in each embryonic stage tested (Figure 2B,C). However, there were a
252 few common genes similarly regulated across each developmental stage. Interestingly,
253 E18 lung mesenchymal cells had a reduced LPS response compared to E11 and E15 cells.
254 Gene Ontology (GO) composition of the gene list of differential expressed genes at 4
255 hours was processed by treemap analysis (REVIGO). The categories of genes regulated
256 by LPS in fetal lung mesenchymal cells were consistent with a predominantly pro-
257 inflammatory innate immune response (Figure 2D)(62). These data showed that fetal lung
258 mesenchymal cells indeed mount an early inflammatory response to LPS. However the
259 genome-wide response could vary depending on the developmental time point from
260 which the cells were isolated.
261
262 The differences in the LPS response that we measured in cells from different embryonic
263 stages could result from changes in the innate immune cellular machinery. Within our
264 mesenchymal cell dataset, we specifically analyzed expression of pattern recognition
265 receptors, innate immune signaling components, transcription factors implicated in
266 inflammation-mediated changes in gene expression, and soluble inflammatory mediators.
267 Figure 3 shows some of the different repertoires of microbial product receptors in each
268 cell line. The LPS receptor *Tlr4* was most highly expressed in E15 cells. LPS induced
269 expression of multiple receptors including *Tlr2* and *Tlr3* in E11 and E15 cells, but not in
270 E18 cells. *Tlr6* expression was highest in E11 cells. Interestingly, *Clec2e*, *Tlr5,* and

Nalp2 were each enriched in E18 cells. Under control conditions, E18 mesenchymal cells had more abundant expression of *Irak2*, *Traf5*, *Akt1*, *Atf5*, *Prkcd, Chuk (Ikk-alpha)*, and *Map2k4*. Additionally, the LPS induction of *Nfkb1*, *Myd88*, *Ikbke*, *Map3k8*, *Ikbkap*, *Cepbd,* and *Nfkbia*, was lower in E18 cells. Genes from the CC and CXC family of chemokines were highly induced by LPS treatment. Interestingly, *Ccl5*, *Cxcl5*, *Cxcl16*, and *Cxcl10* were not as increased following LPS treatment in E18 cells compared to E11 and E15 samples.

To better understand how longer exposure to inflammation might affect lung mesenchymal cell function, we next investigated time-dependent changes in gene expression (Figure 4). Analyzing the data from E15 cells, we found fewer numbers of genes increased by 24 h and 48 h of LPS treatment compared to the early 4 h response (Figure 4A,B). Slightly fewer genes were still downregulated at 48 h of LPS treatment (Figure 4C). Interestingly, analysis of the differentially expressed genes following 48 h of treatment generated a different set of ontologies compared to early response genes (Figure 4D). These data suggested that later changes in mesenchymal cell gene expression could be less related to microbial sensing and more consistent with broader alterations in biological function. The differences measured in genes along the innate immune response pathway at different stages of development were relatively stable over time following LPS treatment (Figure 5). Similar to the patterns measured 4 h following LPS treatment, E18 mesenchymal cells expressed a unique pattern of innate immune receptors, signaling components, and soluble mediators both under control conditions and up to 48 h following LPS exposure.

Inflammatory signals disrupt expression of multiple genes in fetal lung mesenchymal cells. These changes could represent a global phenotypic shift in mesenchymal cells exposed to inflammation. To identify transcriptional targets in the lung mesenchyme altered by more prolonged inflammatory exposure, we focused on genes inhibited by 48 h of LPS exposure. LPS inhibited expression of nine genes in each of the lines tested (Figure 6A). Expression of these genes correlated with each other, as illustrated in Figures 6B-D. The patterns of expression suggest these genes may be part of an overall LPS-sensitive transcriptional program within lung mesenchymal cells. We particularly noted that LPS inhibited expression of the VEGF receptor *Vegfr2*, also known as *Kdr* or *Flk-1*. While VEGF signaling is known to be critical for normal lung vascular formation and structural alveolar development, the potential role of VEGF signaling in mesenchymal cells is less well understood.

We confirmed the LPS effect on *Vegfr2* expression in E18 primary lung mesenchymal cells from C57BL/6 mice (Figure 7A,B). In these cells, LPS induced expression of *Ccl2* (included as a positive control) and inhibited expression of *Vegfr2* (but did not significantly affect expression of the alternative VEGF receptor *Vegfr1*. We then compared the changes in *Vegfr2* expression in fetal lung mesenchymal cell lines isolated at different developmental stages (Figure 7B). LPS increased *Ccl20* expression in each cell line tested, had no effect on *Vegfr1,* but consistently decreased *Vegfr2* expression. *Vegfr2* has primarily been characterized within vascular endothelia in respect to its role in mediating angiogenesis. To assess potential *Vegfr2* expression in mesenchymal cell

populations, we queried publically available human microarray data sets using the BooleanNet tool (57). We specifically interrogated datasets measuring *VEGFR2* and the endothelial-specific genes *CDH5* (VE-cadherin) and *PECAM-1* (CD31). Most samples with *VEGFR2* expression also expressed *CDH5* (Figure 7C). However, a subset of samples expressed *VEGFR2* with only background levels of *CDH5* (expanded in rectangle). Samples indicated in red were from mesenchymal cells or mesenchymal stromal cells. Similar results were obtained when comparing *PECAM-1* and *VEGFR2* expression across the same data sets. The majority of samples expressing *VEGFR2* also expressed *PECAM-1*, however a small subset of samples that included mesenchymal cells expressed *VEGFR2* without *PECAM-1*. To obtain a better understanding of what genes might be co-expressed with *Vegfr2* in fetal lung mesenchyme, we interrogated our original gene expression dataset to identify genes whose expression was most highly correlated with *Vegfr2*, independent of cell line or LPS treatment (Figure 7D). In addition to *Ahr* and *Csdc2* identified in Figure 6, we also identified *Smad6* and *Smad9*, both inhibitors of BMP signaling (48, 63). The tumor suppressor gene *Pdgfrl* (26, 35) had the highest correlation with *Vegfr2* expression. These genes may comprise a global expression program in fetal lung mesenchymal cells that includes *Vegfr2*.

In vascular endothelial cells, VEGF signaling through VEGFR2 stimulates angiogenesis by increasing directed cell migration and proliferation. To test if LPS-mediated reduction in *Vegfr2* expression led to functional changes in fetal lung mesenchymal cells, we performed in vitro wound-healing assays. Closure of artificially induced “wounds” using serum-free media with growth factor addition typically involves collective cell migration

with potential contribution by proliferation (Figure 8A). LPS reduced the area of wound closure when measured after 30 h (Figure 8B). Knockdown of either *Vegfr1* or *Vegfr2* using RNAi demonstrated that *Vegfr2* knockdown (but not *Vegfr1*) reduced the wound closure response to recombinant VEGF-A (Figure 8C). Therefore both LPS and *Vegfr2* knockdown reduced mesenchymal cell wound healing in vitro.

We next measured the effect of LPS on phosphorylation events downstream of VEGFR2. LPS reduced the phosphorylation of VEGFR2, ERK1/2, and AKT following VEGF-A treatment (Figure 9A,B). After AKT activation, the transcriptional response to VEGF is associated with FOXO3A exclusion from the nucleus (1, 14, 60). While VEGF-A treatment of fetal lung mesenchymal cells stimulated FOXO3A exclusion (Figure 9C), FOXO3A appeared to remain localized to the nucleus when cells were first treated with LPS prior to VEGF-A exposure. To quantify this process, we measured the fluorescence intensity of FOXO3A within cell nuclei. Cells pretreated with LPS had increased nuclear FOXO3A following VEGF-A treatment compared to control cells ($*p < 0.001$; n = 29). LPS had no effect on FOXO3A nuclear exclusion following PDGF treatment. Collectively, these data show that fetal lung mesenchymal cells do respond to VEGF-A and that LPS can inhibit this response at least in part by reducing *Vegfr2* expression and subsequent signaling.

Because lung epithelial cells express VEGF (13, 24, 37), we hypothesized that changes in mesenchymal VEGFR2 activity could affect epithelial-mesenchymal interactions important for alveolar development. To test this hypothesis, we used an epithelial-

mesenchymal co-culture model with non-immortalized E15 fetal mouse lung mesenchyme and A549 epithelial cells. We had previously developed this in vitro model to study the cell signaling mechanisms and dynamics leading to 3-dimensional structures during alveolar septa formation (24). Neither A549 cells cultured alone (Figure 10B) nor E15 fetal lung mesenchymal cells cultured with recombinant VEGFA (Figure 10C) formed 3-dimensional structures visible by dark field microscopy. Under control conditions, epithelial-mesenchymal co-cultures form visible 3-dimensional peaks and ridges (Figure 10D). LPS reduced both the formation of peaks and their height (Figure 10E). Similar results were measured when mesenchymal cell cultures were pre-treated with the inhibitors AZD1217 and MGCD265, both of which inhibit the tyrosine kinase activity of VEGFR2 (Figure 10F-K). As A549 cells constitutively express VEGF-A (13), these experiments are consistent with VEGFR2 signaling mediating 3-dimensional epithelial-mesenchymal peak formation.

DISCUSSION

Within the developing lung, mesenchymal cells contribute to alveolar development, wound healing, perivascular regulation, and structural support (43, 44). Abnormal mesenchymal cell differentiation and/or function may contribute to bronchopulmonary dysplasia and other chronic pediatric lung diseases (2, 16). While infection and inflammation likely play a key role in BPD pathogenesis, how mesenchymal cell populations participate in the immune response has been unclear. Our data presented here characterize the fetal lung mesenchymal cell transcriptional response to the bacterial TLR4 ligand LPS. Members of the CC and CXC chemokine families were notably represented in the group of soluble mediator genes increased by LPS exposure. These results provide a detailed transcriptional dataset through which the unique features of the lung mesenchymal innate immune response might be compared to other cell populations.

Identifying the molecular response to inflammation within mesenchymal cells may be key for understanding their role in lung disease. In response to inhaled pathogens, lung macrophages, eosinophils, and neutrophils likely generate the initial inflammatory response and injury (56). Similarly, lymphocytes and dendritic cells likely play key roles in allergic lung disease and asthma (22). However, mesenchymal cell populations may regulate the immune response and promote wound healing. In the immature and developing lung, mesenchymal cells have many of the same properties as mesenchymal stromal cells that have been explored for their various therapeutic possibilities (51). The anti-inflammatory and regenerative properties of mesenchymal stromal cells may be due to the production and release of anti-inflammatory soluble mediators (29). However, we

show here that developing lung mesenchymal cells do mount an innate immune response to LPS. Many of the genes increased by LPS in fetal lung mesenchymal cells are commonly induced as part of the innate immune response. However the overall response profile is weighted toward a subset of chemokines and antimicrobial genes. Importantly, our studies here were focused on defining the innate immune response specifically in fetal lung mesenchymal cells. The in vitro models and cells tested do not take into account how additional cell populations in the lung could affect how mesenchymal cells respond to microbial stimuli and inflammatory mediators in vivo.

Microbial products and inflammatory mediators can disrupt expression of multiple genes critical for lung development. While macrophages in the fetal and neonatal lung appear to be the major cellular site of inflammatory activation and cytokine release, macrophage-derived soluble mediators target the other cell populations in the lung (10). In ovine studies, LPS inhibited *Shh* expression and disrupted normal expression of *Wnt1*, *Wnt4*, and *Wnt7b* (20, 38). Prolonged exposure of developing lambs to either LPS or Ureaplasma led to reduced TGFβ signaling, which plays a significant role in lung morphogenesis (19). In experimental mouse models, inflammatory signaling inhibited expression of *Itga8*, *Fgf10*, *Bmp4*, and *Bmpr1a*, each critical for normal lung development (5-7). The observations that inflammation inhibits multiple genes important for lung development suggest inflammatory signaling could have global effects on developmental transcription within the immature lung. Interestingly, the transcriptional profile was different in the cell lines isolated from different stages of fetal lung development. As the cell lines tested are likely heterogeneous representations of

mesenchymal cells in the lung at each stage, additional studies will need to characterize how the immune response is developmentally regulated in the various cell populations within the lung.

Our results begin to better characterize the connections between inflammation and alterations in lung development. When considered separately, the molecular pathways regulating lung development and the innate immune system are well detailed. Understanding how inflammation can disrupt development requires dissecting how these pathways intersect. In the fetal lung mesenchyme, inflammatory signaling alters expression of genes critical for development. Our data here identify two genes important for development, *Vegfr2* and *Hs6st1* (53), which are inhibited by LPS treatment. We have previously shown that NF-κB-Sp3 interactions inhibit normal *Fgf10* expression (5, 15), leading to changes in other downstream genes including *Bmp4* and *Bmpr1a* (7). Inflammation also inhibits expression of the $\alpha_8\beta_1$ integrin, which is critical for normal mesenchymal cell migration and membrane dynamics during lung formation (6). Recent work has demonstrated that lung epithelial IKKβ activity can disrupt elastin synthesis and organization at the alveolar level (8). The multiple developmental targets of inflammation suggest that innate immune pathways may target global transcriptional programs within specific cell populations. In addition, the mechanisms leading to inhibition of gene expression may be more diverse and complex than transcriptional activation. The data presented here may help better characterize these genome-wide effects.

In endothelial cells, VEGF signaling through VEGFR2 promotes angiogenesis and alveolar capillary formation (50). Our data show that fetal lung mesenchymal cells also express VEGFR2. We do not yet know the relative contribution of changes in VEGFR2 expression to inflammation-mediated lung injury or abnormal lung development. However, the data presented here suggest a role for VEGF signaling in non-endothelial mesenchymal populations. As in vascular endothelia (1, 14, 60), VEGF signaling in mesenchymal cells activates the ERK/AKT pathway, stimulates mesenchymal cell migration, and stimulates changes in FOXO3A subcellular localization. Interestingly, siRNA mediated *Vegfr2* knockdown led to reduced migration following VEGF-A administration (Figure 7). Because VEGFR1 can function as a high-affinity decoy receptor, decreased VEGFR2 relative to VEGFR1 could lead to reduce cell migration (23, 50). While the mesenchymal cells studied here potentially represent endothelial precursor cells (66), they do not express other vascular endothelial markers under typical culture conditions. In addition, our analyses of published human expression datasets clearly show *VEGFR2* expression in cells that do not express the endothelial markers *CDH5* or *PECAM1*. As many of these samples are from mesenchymal or mesenchymal stromal cell populations, VEGFR2 may represent an important growth factor receptor in mesenchymal cell populations in addition to its role in vascular biology.

As new alveolar capillaries form, vascular endothelial cells respond to VEGF released by alveolar epithelial cells and migrate more closely to the epithelial basement membrane (9, 28). The intimate relationship of alveolar epithelia with capillary endothelial cells reduces the potential spatial barrier to gas exchange. Mesenchymal-derived pericytes are also part

of this complex multicellular unit, potentially providing structural support and maintenance to the alveolar capillary unit (45, 59). VEGF signaling might guide parallel migration of mesenchymal pericytes alongside vascular endothelial cells during capillary development. Interestingly, PDGF signaling also targets mesenchymal cells in the developing alveolus, driving alveolar myofibroblast differentiation and migration (11, 12). Our in vitro data show LPS inhibits the response to VEGF by reducing *Vegfr2* expression while not affecting the response to PDGF. As both VEGF and PDGF are required for normal alveolar formation, shifting the response toward PDGF while reducing VEGF sensitivity could skew the normal alveolar architecture in premature lungs exposed to inflammation.

REFERENCES

1. **Abid MR, Yano K, Guo S, Patel VI, Shrikhande G, Spokes KC, Ferran C, and Aird WC**. Forkhead transcription factors inhibit vascular smooth muscle cell proliferation and neointimal hyperplasia. *J Biol Chem* 280: 29864-29873, 2005.

2. **Ahlfeld SK, and Conway SJ**. Aberrant signaling pathways of the lung mesenchyme and their contributions to the pathogenesis of bronchopulmonary dysplasia. *Birth Defects Res A Clin Mol Teratol* 94: 3-15, 2012.

3. **Al Alam D, El Agha E, Sakurai R, Kheirollahi V, Moiseenko A, Danopoulos S, Shrestha A, Schmoldt C, Quantius J, Herold S, Chao CM, Tiozzo C, De Langhe S, Plikus MV, Thornton M, Grubbs B, Minoo P, Rehan VK, and Bellusci S**. Evidence for the involvement of fibroblast growth factor 10 in lipofibroblast formation during embryonic lung development. *Development* 142: 4139-4150, 2015.

4. **Baker CD, and Alvira CM**. Disrupted lung development and bronchopulmonary dysplasia: opportunities for lung repair and regeneration. *Curr Opin Pediatr* 26: 306-314, 2014.

5. **Benjamin JT, Carver BJ, Plosa EJ, Yamamoto Y, Miller JD, Liu JH, van der Meer R, Blackwell TS, and Prince LS**. NF-kappaB activation limits airway branching through inhibition of Sp1-mediated fibroblast growth factor-10 expression. *J Immunol* 185: 4896-4903, 2010.

6. **Benjamin JT, Gaston DC, Halloran BA, Schnapp LM, Zent R, and Prince LS**. The role of integrin alpha8beta1 in fetal lung morphogenesis and injury. *Dev Biol* 335: 407-417, 2009.

7. **Benjamin JT, Smith RJ, Halloran BA, Day TJ, Kelly DR, and Prince LS**. FGF-10 is decreased in bronchopulmonary dysplasia and suppressed by Toll-like receptor activation. *Am J Physiol Lung Cell Mol Physiol* 292: L550-558, 2007.

8. **Benjamin JT, van der Meer R, Im AM, Plosa EJ, Zaynagetdinov R, Burman A, Havrilla ME, Gleaves LA, Polosukhin VV, Deutsch GH, Yanagisawa H, Davidson JM, Prince LS, Young LR, and Blackwell TS**. Epithelial-Derived Inflammation Disrupts Elastin Assembly and Alters Saccular Stage Lung Development. *Am J Pathol* 186: 1786-1800, 2016.

9. **Bhatt AJ, Amin SB, Chess PR, Watkins RH, and Maniscalco WM**. Expression of vascular endothelial growth factor and Flk-1 in developing and glucocorticoid-treated mouse lung. *Pediatr Res* 47: 606-613, 2000.

10. **Blackwell TS, Hipps AN, Yamamoto Y, Han W, Barham WJ, Ostrowski MC, Yull FE, and Prince LS**. NF-kappaB signaling in fetal lung macrophages disrupts airway morphogenesis. *J Immunol* 187: 2740-2747, 2011.

11. **Bostrom H, Gritli-Linde A, and Betsholtz C**. PDGF-A/PDGF alpha-receptor signaling is required for lung growth and the formation of alveoli but not for early lung branching morphogenesis. *Dev Dyn* 223: 155-162, 2002.

12. **Bostrom H, Willetts K, Pekny M, Leveen P, Lindahl P, Hedstrand H, Pekna M, Hellstrom M, Gebre-Medhin S, Schalling M, Nilsson M, Kurland S, Tornell J, Heath JK, and Betsholtz C**. PDGF-A signaling is a critical event in lung alveolar myofibroblast development and alveogenesis. *Cell* 85: 863-873, 1996.

13. **Boussat S, Eddahibi S, Coste A, Fataccioli V, Gouge M, Housset B, Adnot S, and Maitre B**. Expression and regulation of vascular endothelial growth factor in human pulmonary epithelial cells. *Am J Physiol Lung Cell Mol Physiol* 279: L371-378, 2000.

14. **Brunet A, Bonni A, Zigmond MJ, Lin MZ, Juo P, Hu LS, Anderson MJ, Arden KC, Blenis J, and Greenberg ME**. Akt promotes cell survival by phosphorylating and inhibiting a Forkhead transcription factor. *Cell* 96: 857-868, 1999.

15. **Carver BJ, Plosa EJ, Stinnett AM, Blackwell TS, and Prince LS**. Interactions between NF-kappaB and SP3 connect inflammatory signaling with reduced FGF-10 expression. *J Biol Chem* 288: 15318-15325, 2013.

16. **Chao CM, El Agha E, Tiozzo C, Minoo P, and Bellusci S**. A breath of fresh air on the mesenchyme: impact of impaired mesenchymal development on the pathogenesis of bronchopulmonary dysplasia. *Front Med (Lausanne)* 2: 27, 2015.

17. **Chao CM, Moiseenko A, Zimmer KP, and Bellusci S**. Alveologenesis: key cellular players and fibroblast growth factor 10 signaling. *Mol Cell Pediatr* 3: 17, 2016.

18. **Cohen ED, Ihida-Stansbury K, Lu MM, Panettieri RA, Jones PL, and Morrisey EE**. Wnt signaling regulates smooth muscle precursor development in the mouse lung via a tenascin C/PDGFR pathway. *J Clin Invest* 119: 2538-2549, 2009.

19. **Collins JJ, Kallapur SG, Knox CL, Kemp MW, Kuypers E, Zimmermann LJ, Newnham JP, Jobe AH, and Kramer BW**. Repeated intrauterine exposures to inflammatory stimuli attenuated transforming growth factor-beta signaling in the ovine fetal lung. *Neonatology* 104: 49-55, 2013.

20. **Collins JJ, Kuypers E, Nitsos I, Jane Pillow J, Polglase GR, Kemp MW, Newnham JP, Cleutjens JP, Frints SG, Kallapur SG, Jobe AH, and Kramer BW**.

LPS-induced chorioamnionitis and antenatal corticosteroids modulate Shh signaling in the ovine fetal lung. *Am J Physiol Lung Cell Mol Physiol* 303: L778-787, 2012.

21. **Dieperink HI, Blackwell TS, and Prince LS**. Hyperoxia and apoptosis in developing mouse lung mesenchyme. *Pediatr Res* 59: 185-190, 2006.

22. **Fahy JV**. Type 2 inflammation in asthma--present in most, absent in many. *Nat Rev Immunol* 15: 57-65, 2015.

23. **Fong GH, Rossant J, Gertsenstein M, and Breitman ML**. Role of the Flt-1 receptor tyrosine kinase in regulating the assembly of vascular endothelium. *Nature* 376: 66-70, 1995.

24. **Greer RM, Miller JD, Okoh VO, Halloran BA, and Prince LS**. Epithelial-mesenchymal co-culture model for studying alveolar morphogenesis. *Organogenesis* 10: 340-349, 2014.

25. **Greer RM, Peyton M, Larsen JE, Girard L, Xie Y, Gazdar AF, Harran P, Wang L, Brekken RA, Wang X, and Minna JD**. SMAC mimetic (JP1201) sensitizes non-small cell lung cancers to multiple chemotherapy agents in an IAP-dependent but TNF-alpha-independent manner. *Cancer Res* 71: 7640-7648, 2011.

26. **Guo FJ, Zhang WJ, Li YL, Liu Y, Li YH, Huang J, Wang JJ, Xie PL, and Li GC**. Expression and functional characterization of platelet-derived growth factor receptor-like gene. *World J Gastroenterol* 16: 1465-1472, 2010.

27. **Hines EA, and Sun X**. Tissue crosstalk in lung development. *J Cell Biochem* 115: 1469-1477, 2014.

28. **Hislop A**. Developmental biology of the pulmonary circulation. *Paediatr Respir Rev* 6: 35-43, 2005.

29. **Ho MS, Mei SH, and Stewart DJ**. The Immunomodulatory and Therapeutic Effects of Mesenchymal Stromal Cells for Acute Lung Injury and Sepsis. *J Cell Physiol* 230: 2606-2617, 2015.

30. **Huang da W, Sherman BT, and Lempicki RA**. Bioinformatics enrichment tools: paths toward the comprehensive functional analysis of large gene lists. *Nucleic acids research* 37: 1-13, 2009.

31. **Huang da W, Sherman BT, and Lempicki RA**. Systematic and integrative analysis of large gene lists using DAVID bioinformatics resources. *Nature protocols* 4: 44-57, 2009.

32. **Husain AN, Siddiqui NH, and Stocker JT**. Pathology of arrested acinar development in postsurfactant bronchopulmonary dysplasia. *Hum Pathol* 29: 710-717, 1998.

33. **Jat PS, Noble MD, Ataliotis P, Tanaka Y, Yannoutsos N, Larsen L, and Kioussis D**. Direct derivation of conditionally immortal cell lines from an H-2Kb-tsA58 transgenic mouse. *Proc Natl Acad Sci U S A* 88: 5096-5100, 1991.

34. **Kim N, and Vu TH**. Parabronchial smooth muscle cells and alveolar myofibroblasts in lung development. *Birth Defects Res C Embryo Today* 78: 80-89, 2006.

35. **Kim YW, Yun SJ, Jeong P, Kim SK, Kim SY, Yan C, Seo SP, Lee SK, Kim J, and Kim WJ**. The c-MET Network as Novel Prognostic Marker for Predicting Bladder Cancer Patients with an Increased Risk of Developing Aggressive Disease. *PLoS One* 10: e0134552, 2015.

36. **Kumar ME, Bogard PE, Espinoza FH, Menke DB, Kingsley DM, and Krasnow MA**. Mesenchymal cells. Defining a mesenchymal progenitor niche at single-cell resolution. *Science* 346: 1258810, 2014.

37. **Kumar VH, and Ryan RM**. Growth factors in the fetal and neonatal lung. *Front Biosci* 9: 464-480, 2004.

38. **Kuypers E, Willems MG, Collins JJ, Wolfs TG, Nitsos I, Jane Pillow J, Polglase GR, Kemp MW, Newnham JP, Delhaas T, Jobe AH, Kallapur SG, and Kramer BW**. Altered canonical Wingless-Int signaling in the ovine fetal lung after exposure to intra-amniotic lipopolysaccharide and antenatal betamethasone. *Pediatr Res* 75: 281-287, 2014.

39. **Li A, Ma S, Smith SM, Lee MK, Fischer A, Borok Z, Bellusci S, Li C, and Minoo P**. Mesodermal ALK5 controls lung myofibroblast versus lipofibroblast cell fate. *BMC Biol* 14: 19, 2016.

40. **Li C, Li M, Li S, Xing Y, Yang CY, Li A, Borok Z, De Langhe S, and Minoo P**. Progenitors of secondary crest myofibroblasts are developmentally committed in early lung mesoderm. *Stem Cells* 33: 999-1012, 2015.

41. **Livak KJ, and Schmittgen TD**. Analysis of relative gene expression data using real-time quantitative PCR and the 2(-DDC(T)) Method. *Methods* 25: 402-408, 2001.

42. **Madurga A, Mizikova I, Ruiz-Camp J, and Morty RE**. Recent advances in late lung development and the pathogenesis of bronchopulmonary dysplasia. *Am J Physiol Lung Cell Mol Physiol* 305: L893-905, 2013.

43. **Mariani TJ**. Update on Molecular Biology of Lung Development--Transcriptomics. *Clin Perinatol* 42: 685-695, 2015.

612 44. **McCulley D, Wienhold M, and Sun X**. The pulmonary mesenchyme directs
613 lung development. *Curr Opin Genet Dev* 32: 98-105, 2015.
614 45. **McGowan SE**. Paracrine cellular and extracellular matrix interactions with
615 mesenchymal progenitors during pulmonary alveolar septation. *Birth Defects Res A Clin*
616 *Mol Teratol* 100: 227-239, 2014.
617 46. **Miller LA, Wert SE, Clark JC, Xu Y, Perl AK, and Whitsett JA**. Role of
618 Sonic hedgehog in patterning of tracheal-bronchial cartilage and the peripheral lung. *Dev*
619 *Dyn* 231: 57-71, 2004.
620 47. **Morrisey EE, Cardoso WV, Lane RH, Rabinovitch M, Abman SH, Ai X,**
621 **Albertine KH, Bland RD, Chapman HA, Checkley W, Epstein JA, Kintner CR,**
622 **Kumar M, Minoo P, Mariani TJ, McDonald DM, Mukouyama YS, Prince LS, Reese**
623 **J, Rossant J, Shi W, Sun X, Werb Z, Whitsett JA, Gail D, Blaisdell CJ, and Lin QS**.
624 Molecular determinants of lung development. *Ann Am Thorac Soc* 10: S12-16, 2013.
625 48. **Mouillesseaux KP, Wiley DS, Saunders LM, Wylie LA, Kushner EJ, Chong**
626 **DC, Citrin KM, Barber AT, Park Y, Kim JD, Samsa LA, Kim J, Liu J, Jin SW, and**
627 **Bautch VL**. Notch regulates BMP responsiveness and lateral branching in vessel
628 networks via SMAD6. *Nat Commun* 7: 13247, 2016.
629 49. **Ochs M, Nyengaard JR, Jung A, Knudsen L, Voigt M, Wahlers T, Richter J,**
630 **and Gundersen HJ**. The number of alveoli in the human lung. *Am J Respir Crit Care*
631 *Med* 169: 120-124, 2004.
632 50. **Olsson AK, Dimberg A, Kreuger J, and Claesson-Welsh L**. VEGF receptor
633 signalling - in control of vascular function. *Nat Rev Mol Cell Biol* 7: 359-371, 2006.

634 51. **Pierro M, Ciarmoli E, and Thebaud B**. Bronchopulmonary Dysplasia and
635 Chronic Lung Disease: Stem Cell Therapy. *Clin Perinatol* 42: 889-910, 2015.
636 52. **Prince LS, Dieperink HI, Okoh VO, Fierro-Perez GA, and Lallone RL**. Toll-
637 like receptor signaling inhibits structural development of the distal fetal mouse lung. *Dev*
638 *Dyn* 233: 553-561, 2005.
639 53. **Qu X, Carbe C, Tao C, Powers A, Lawrence R, van Kuppevelt TH, Cardoso**
640 **WV, Grobe K, Esko JD, and Zhang X**. Lacrimal gland development and Fgf10-Fgfr2b
641 signaling are controlled by 2-O- and 6-O-sulfated heparan sulfate. *J Biol Chem* 286:
642 14435-14444, 2011.
643 54. **Ritchie ME, Phipson B, Wu D, Hu Y, Law CW, Shi W, and Smyth GK**.
644 limma powers differential expression analyses for RNA-sequencing and microarray
645 studies. *Nucleic Acids Res* 43: e47, 2015.
646 55. **Ritchie ME, Phipson B, Wu D, Hu Y, Law CW, Shi W, and Smyth GK**.
647 limma powers differential expression analyses for RNA-sequencing and microarray
648 studies. *Nucleic acids research* 2015.
649 56. **Robb CT, Regan KH, Dorward DA, and Rossi AG**. Key mechanisms
650 governing resolution of lung inflammation. *Semin Immunopathol* 2016.
651 57. **Sahoo D, Dill DL, Gentles AJ, Tibshirani R, and Plevritis SK**. Boolean
652 implication networks derived from large scale, whole genome microarray datasets.
653 *Genome Biol* 9: R157, 2008.
654 58. **Shannon JM, and Hyatt BA**. Epithelial-mesenchymal interactions in the
655 developing lung. *Annu Rev Physiol* 66: 625-645, 2004.

59. **Sirianni FE, Chu FS, and Walker DC**. Human alveolar wall fibroblasts directly link epithelial type 2 cells to capillary endothelium. *Am J Respir Crit Care Med* 168: 1532-1537, 2003.

60. **Skurk C, Maatz H, Kim HS, Yang J, Abid MR, Aird WC, and Walsh K**. The Akt-regulated forkhead transcription factor FOXO3a controls endothelial cell viability through modulation of the caspase-8 inhibitor FLIP. *J Biol Chem* 279: 1513-1525, 2004.

61. **Smyth GK**. Linear models and empirical bayes methods for assessing differential expression in microarray experiments. *Stat Appl Genet Mol Biol* 3: Article3, 2004.

62. **Supek F, Bošnjak M, Škunca N, and Šmuc T**. REVIGO Summarizes and Visualizes Long Lists of Gene Ontology Terms. *PLoS ONE* 6: e21800, 2011.

63. **Tsukamoto S, Mizuta T, Fujimoto M, Ohte S, Osawa K, Miyamoto A, Yoneyama K, Murata E, Machiya A, Jimi E, Kokabu S, and Katagiri T**. Smad9 is a new type of transcriptional regulator in bone morphogenetic protein signaling. *Sci Rep* 4: 7596, 2014.

64. **White AC, Lavine KJ, and Ornitz DM**. FGF9 and SHH regulate mesenchymal Vegfa expression and development of the pulmonary capillary network. *Development* 134: 3743-3752, 2007.

65. **Whitsett JA, and Weaver TE**. Alveolar development and disease. *Am J Respir Cell Mol Biol* 53: 1-7, 2015.

66. **Yamamoto Y, Baldwin HS, and Prince LS**. Endothelial differentiation by multipotent fetal mouse lung mesenchymal cells. *Stem Cells Dev* 21: 1455-1465, 2012.

679 ACKNOWLEDGMENTS

680 We are ever grateful for the helpful comments, advice, and guidance from our colleagues
681 at the University of California, San Diego, Rady Children's Hospital, San Diego, and
682 Vanderbilt University School of Medicine. We also thank the staff of the Vanderbilt
683 Technologies for Advanced Genomics.

684
685

686 FIGURE LEGENDS

687 **Figure 1.** Analysis of effects of LPS on fetal lung mesenchymal cells. (A,B) Primary
688 fetal mouse lung mesenchymal cells from E15 embryos were treated with LPS (250
689 ng/ml) for 24 h. Phase contrast images (20X) show that LPS altered mesenchymal cell
690 morphology, giving rise to more spindle-shaped cells with longer cell processes. (C).
691 Mesenchymal cell lines from E13, E15, and E18 *SV40*^{tsA58} mouse lungs were treated with
692 LPS (250 ng/ml) for 4 h, 24 h, and 48 h. Total RNA was then isolated and gene
693 expression was measured using Affymetrix Mouse Gene 1.0ST microarrays. Each
694 condition and time point was repeated in triplicate. Samples were not pooled. Principal
695 Component Analysis (PCA) of 54 microarray samples identified three groupings based
696 primarily on the gestational ages of mesenchymal cells studied. (D). Heat map showing
697 unsupervised hierarchical clustering analysis was done on both genes and individual
698 experimental time points and replicates using complete linkage analysis. Each vertical
699 column indicates a unique experimental replicate. Experiments clustered by LPS
700 treatment. (E). Differential gene expression analysis between control and LPS-treated
701 samples at all time points identified 490 genes up regulated and 285 genes down
702 regulated by LPS.

703

704 **Figure 2.** Analysis of early response genes following 4 h of LPS treatment. (A).
705 Unsupervised hierarchical clustering analysis of 182 genes differentially expressed after 4
706 hours of LPS treatment. Dendrograms are based on correlation values following complete
707 linkage analysis. Each vertical column indicates a unique experimental replicate. (B,C)
708 Venn diagrams show the number of genes found to be significantly up (B) or down (C)

709 regulated at 4 hours of LPS treatment in E11, E15, and E18 samples. (D). Functional
710 annotation clustering of gene ontology (GO) analysis. Genes with significant changes
711 following 4 h of LPS treatment were categorized using DAVID with GO results
712 visualized using REVIGO TreeMap.
713
714 **Figure 3.** Developmental changes in innate immune response genes. Gene expression
715 data is shown for pattern recognition receptors, signaling components and transcription
716 factors, and soluble inflammatory mediators. Normalized control and 4 h LPS treatment
717 data are shown for each replicate using E11, E15, and E18 cells. Red indicates increased
718 relative gene expression and green/blue indicates decreased relative gene expression.
719 Genes with notable patterns are indicated at right. The LPS receptor *Tlr4* is indicated in
720 red.
721
722 **Figure 4.** Analysis of mesenchymal cell response to LPS over time. (A). Differential
723 gene expression was determined for E15 cells treated with or without LPS. Significant
724 genes were then used in an unsupervised hierarchical clustering analysis. Both genes and
725 arrays were submitted to complete linkage analysis and dendrograms were based on
726 correlation values. Arrays cluster based on treatment and then on treatment time.
727 Differential gene expression was determined using a linear model ($p<0.01$) considering
728 treatment and gestational age. (B,C). Venn diagrams show the number of genes found to
729 be significantly up (B) or down (C) regulated at 4, 24, and 48 hours of LPS treatment.
730 (D). Functional annotation clustering of gene ontology analysis of 150 differentially

731 expressed genes following 48 hours of LPS treatment. GO categories were distinct from
732 those represented in analysis of early response genes.
733
734 **Figure 5.** Developmental changes in innate immune response genes following extended
735 LPS treatment. Gene expression data is shown for pattern recognition receptors, signaling
736 components and transcription factors, and soluble inflammatory mediators. Normalized
737 control and 4 h, 24, and 48 h LPS treatment data are shown for each replicate using E11,
738 E15, and E18 cells. Red indicates increased relative gene expression and green/blue
739 indicates decreased relative gene expression. Genes with notable patterns are indicated at
740 right. The LPS receptor *Tlr4* is indicated in red.
741
742 **Figure 6**. LPS inhibits expression of a core set of mesenchymal genes. (A). Differential
743 gene expression was determined using a linear model (p <0.01) considering gestational
744 age and treatment. Venn diagram shows the number of genes significantly down
745 regulated in E11, E15, and E18 cells, with 9 commonly down regulated genes across all
746 samples. (B-D). Data plotted for pairs of genes down regulated by LPS demonstrate
747 relative expression across all samples. Control samples are indicated in red. LPS-treated
748 samples are indicated in cyan. Gene expression values represent log_2 of relative
749 expression units.
750
751 **Figure 7.** LPS inhibits *Vegfr2* expression. (A). Measurement of *Ccl2*, *Vegfr1*, and *Vegfr2*
752 expression by real time PCR in E18 primary mouse lung mesenchymal cells (*p <
753 0.0001; n = 6-7). (B). LPS treatment reduced VEGFR2 protein levels in E18 primary

754 mouse lung mesenchymal cells as measured by immunoblotting. Expression levels
755 relative to actin normalized to control values (*$p < 0.05$; n = 4). (C). Box plots showing
756 expression of *Ccl20*, *Vegfr1*, and *Vegfr2* in control (ctrl) and LPS treated E11, E15, and
757 E18 mesenchymal cell samples as measured by microarray across all time points tested.
758 (D). Boolean relationships between expression of *CDH5* and *PECAM1* with *VEGFR2*
759 from Affymetrix U133 Plus 2.0 human public datasets using BooleanNet. Correlation of
760 all experimental datasets shown in the left panels. Datasets with *VEGFR2* expression but
761 low *CDH5* or *PECAM1* expression are magnified and shown in right panels. Red crosses
762 indicate samples from mesenchymal cells. (E). All genes detected in the fetal mouse lung
763 mesenchymal dataset were analyzed based on how their expression levels correlated with
764 *Vegfr2*. Genes most highly correlating with *Vegfr2* expression along with their respective
765 correlation coefficients are listed.
766
767 **Figure 8.** VEGF signaling through VEGFR2 stimulated mesenchymal cell migration.
768 (A,B) Artificial wounds were created in confluent monolayers of E15 fetal lung
769 mesenchymal cells. LPS (250 ng/ml) inhibited cell migration as measured by % of
770 closure by cells filling the wound after 30 h (*$p < 0.005$; n = 8). (C). Knockdown of
771 *Vegfr2* expression by siRNA impaired wound healing when VEGF-A was included in the
772 media (*$p < 0.005$; n = 4).
773
774 **Figure 9.** LPS inhibited VEGFR2-mediated signaling in fetal mouse lung mesenchymal
775 cells. E15 primary fetal lung mesenchymal cells were pretreated with LPS for 24 h prior
776 to stimulation with insulin or VEGF-A (10 ng/ml) for 5 min. (A). Lysates were analyzed

by immunoblotting to detect phosphorylation of VEGFR2, ERK1/2, and AKT. (B) Densitometery analysis measuring phosphorylated/total AKT ratios demonstrated that AKT phosphorylation following VEGF-A treatment was lower in cells pretreated with LPS (*$p < 0.05$; n = 4). (C) LPS reduced VEGF-mediated changes in FOXO3A localization. E15 mesenchymal cells were cultured for 24 h in the absence or presence of LPS (250 ng/ml) and then stimulated with either VEGF-A (10 ng/ml) or PDGF-BB (20 ng/ml) for 2 hours. Cells were then fixed, permeabilized, and immunostained for FOXO3A localization. Nuclei were labeled with Draq5. Representative lower power images are shown in the top row and higher magnification of individual cell nuclei are shown below. Nuclear FOXO3a staining was measured and presented as mean nuclear pixel intensity (*$p < 0.001$; n = 29 cells measured from three independent experiments).

Figure 10. LPS and VEGFR2 inhibition disrupted epithelial-mesenchymal interactions. Confluent monolayers of E15 primary fetal mouse lung mesenchymal cells were overlaid with A549 epithelia to form epithelial-mesenchymal co-cultures (A). Following 24 h of co-culture, peaks and ridges form, becoming visible by dark-field microscopy. (B,C). Cultures of only A549 epithelia (A) or E15 mesenchyme treated with recombinant VEGF-A (10 ng/ml) (C) fail to form 3-dimensional structures. (D,E). Seeding A549 cells on confluent monolayers of lung mesenchyme stimulates formation of distinct ridges and peaks. LPS inhibits both the number and height of these structures (E). (F-K). The VEGFR2 tyrosine kinase inhibitors AZD1217 (F,G) and MGCD265 (H,I) reduce both the number ((J), *$p < 0.05$, n = 4) and height ((K), *$p < 0.05$, n = 5) of peaks formed as

799 measured by 3-dimensional laser scanning confocal microscopy. Representative dark-
800 field images shown (5X magnification).

801
802

803 FUNDING INFORMATION

804 This work was supported by the Gerber Foundation (L.S.P.) and National Institutes of

805 Health Grants HL097195 (L.S.P. and T.S.B.), HL086324 (L.S.P), HL116358 (L.S.P and

806 T.S.B.), and HL126703 (L.S.P. and H.M.H.).

807

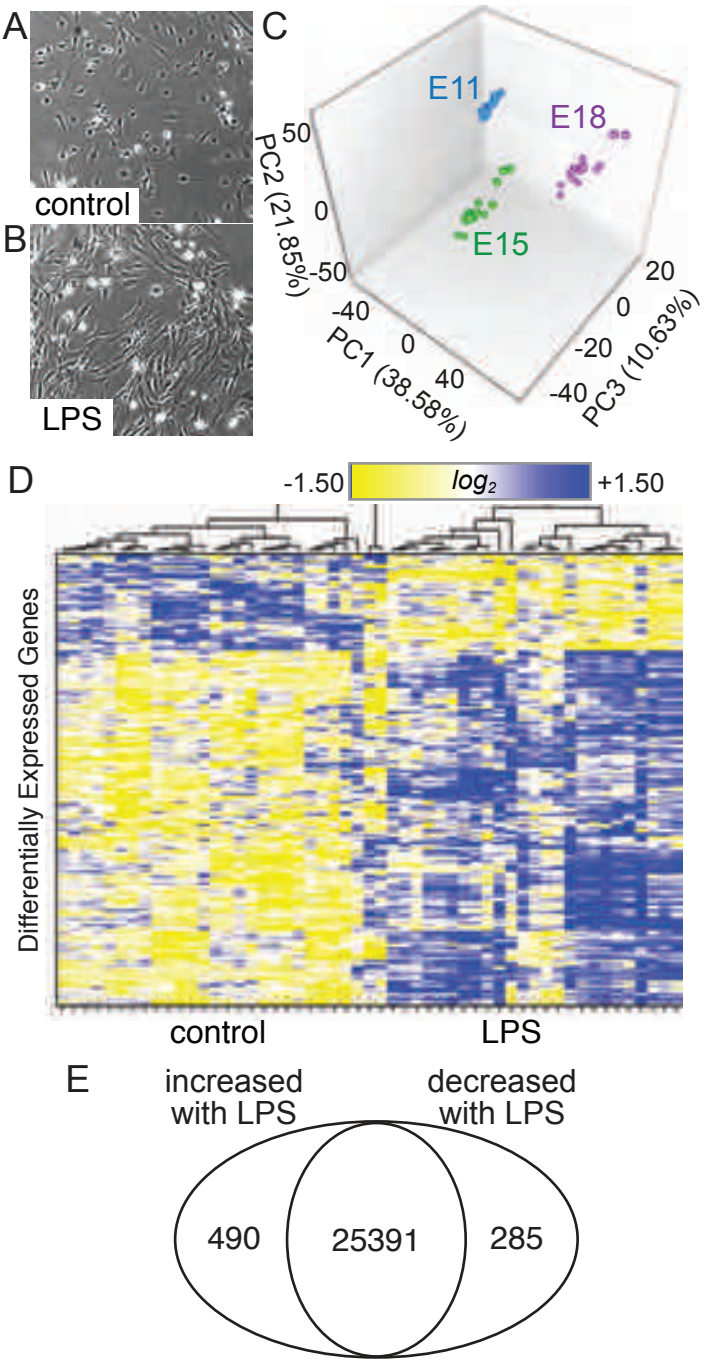
A
control
B
LPS
C
E11
E18
E15
50
0
-50
PC2 (21.85%)
-40
0
40
PC1 (38.58%)
20
0
-20
-40
PC3 (10.63%)
D
-1.50
log2
+1.50
Differentially Expressed Genes
control
LPS
E
increased with LPS
decreased with LPS
490
25391
285

Figure 1

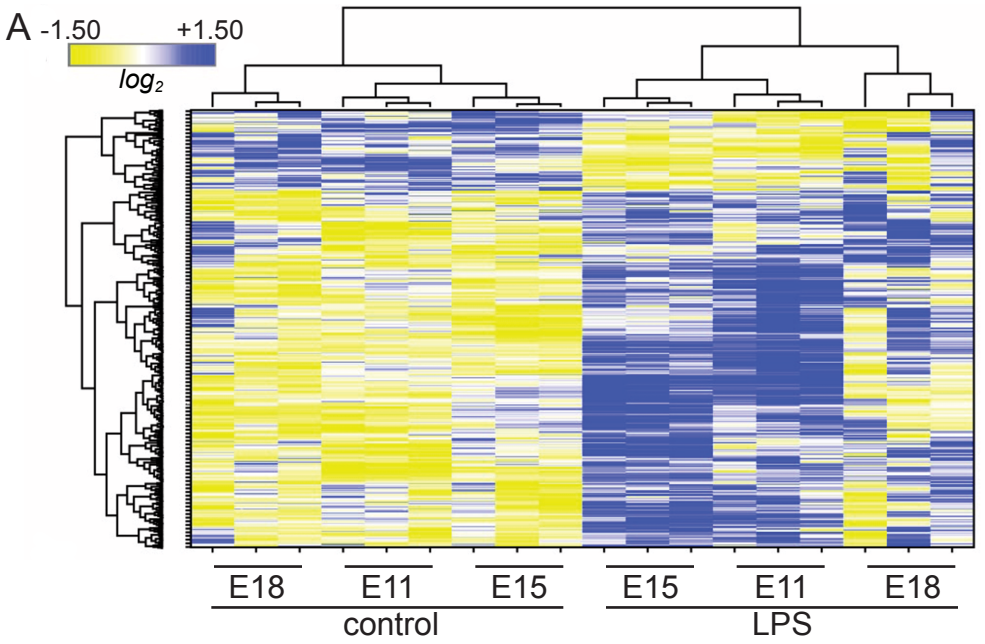
A
-1.50
+1.50
log2
E18
E11
E15
E15
E11
E18
control
LPS

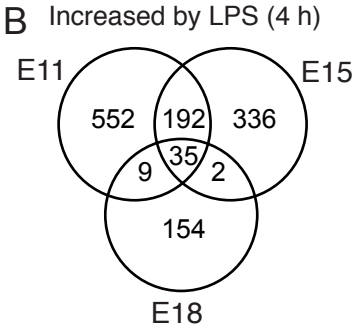
B
Increased by LPS (4 h)
E11
E15
552
192
336
35
9
2
154
E18

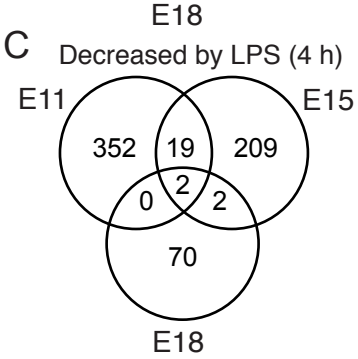
C
Decreased by LPS (4 h)
E11
E15
352
19
209
2
0
2
70
E18

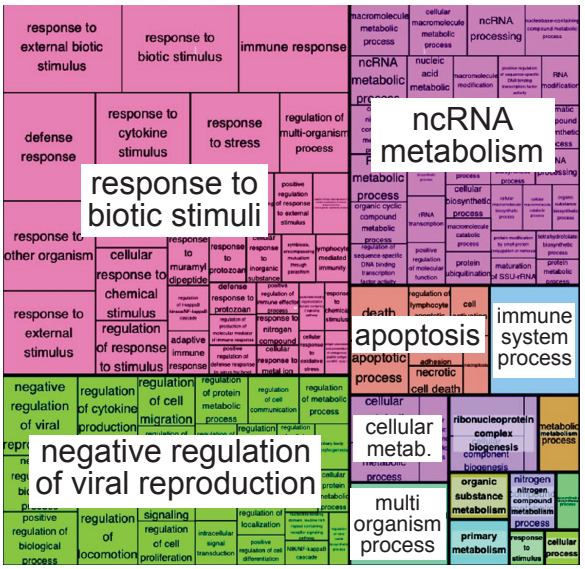
D
response to external biotic stimulus
response to biotic stimulus
immune response
defense response
response to cytokine stimulus
response to stress
regulation of multi-organism process
response to biotic stimuli
response to other organism
cellular response to chemical stimulus
response to external stimulus
regulation of response to stimulus
negative regulation of viral reproduction
positive regulation of biological process
regulation of locomotion
regulation of cell proliferation
ncRNA metabolism
ncRNA processing
nucleic acid metabolic
metabolic process
apoptosis
immune system process
cellular metab.
multi organism process
organic substance metabolism
primary metabolism

Figure 2

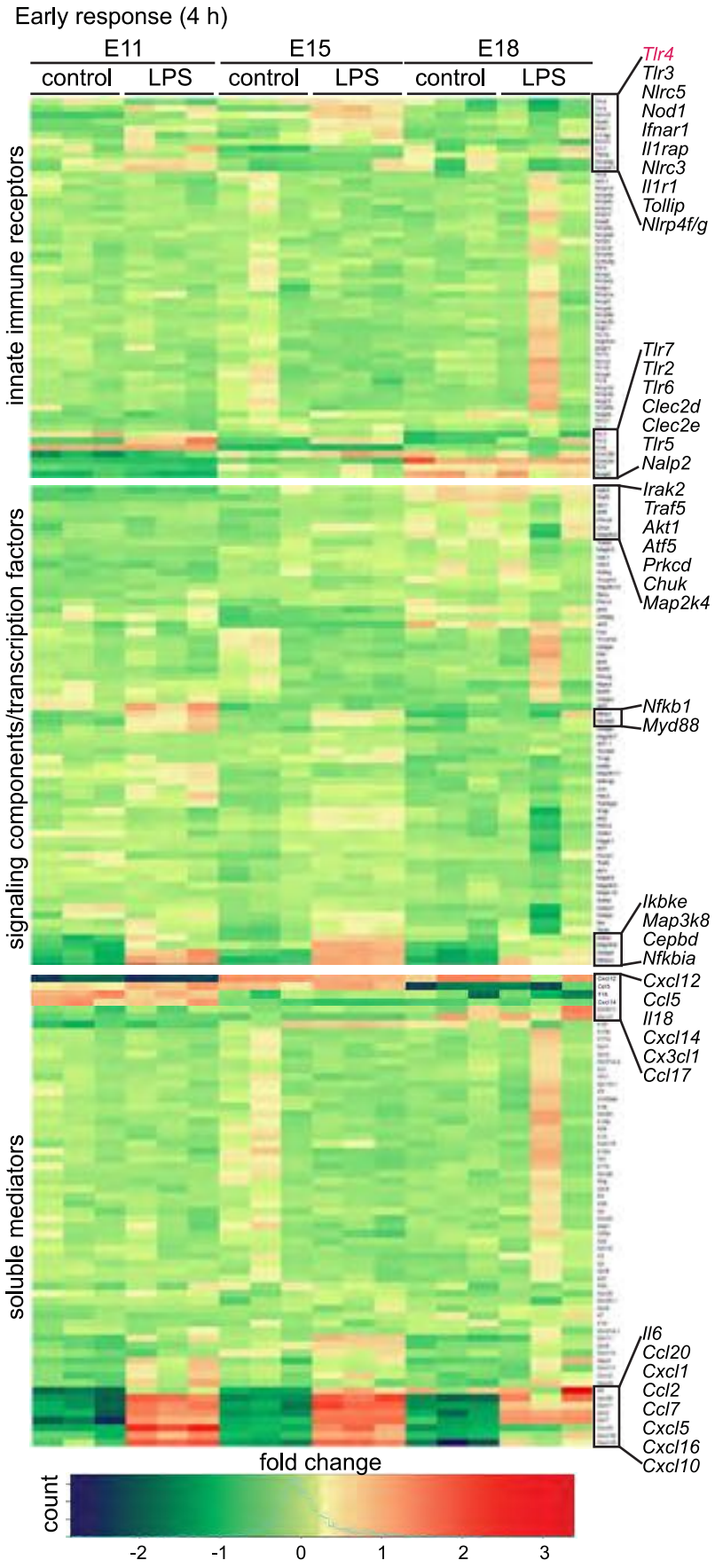
Early response (4 h)
E11
E15
E18
control
LPS
control
LPS
control
LPS
innate immune receptors
signaling components/transcription factors
soluble mediators
Tlr4
Tlr3
Nlrc5
Nod1
Ifnar1
Il1rap
Nlrc3
Il1r1
Tollip
Nlrp4f/g
Tlr7
Tlr2
Tlr6
Clec2d
Clec2e
Tlr5
Nalp2
Irak2
Traf5
Akt1
Atf5
Prkcd
Chuk
Map2k4
Nfkb1
Myd88
Ikbke
Map3k8
Cepbd
Nfkbia
Cxcl12
Ccl5
Il18
Cxcl14
Cx3cl1
Ccl17
Il6
Ccl20
Cxcl1
Ccl2
Ccl7
Cxcl5
Cxcl16
Cxcl10
fold change
count
-2
-1
0
1
2
3

Figure 3

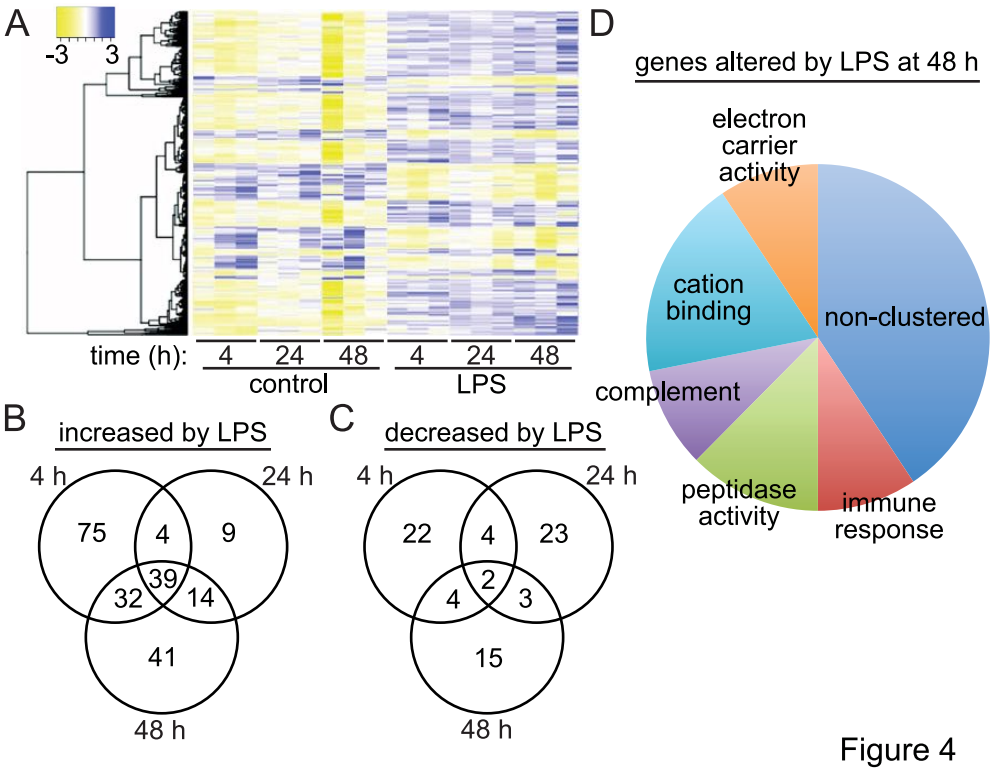
A
-3
3
time (h):
4
24
48
4
24
48
control
LPS
B
increased by LPS
4 h
24 h
75
4
9
39
32
14
41
48 h
C
decreased by LPS
4 h
24 h
22
4
23
2
4
3
15
48 h
D
genes altered by LPS at 48 h
electron carrier activity
cation binding
non-clustered
complement
peptidase activity
immune response

Figure 4

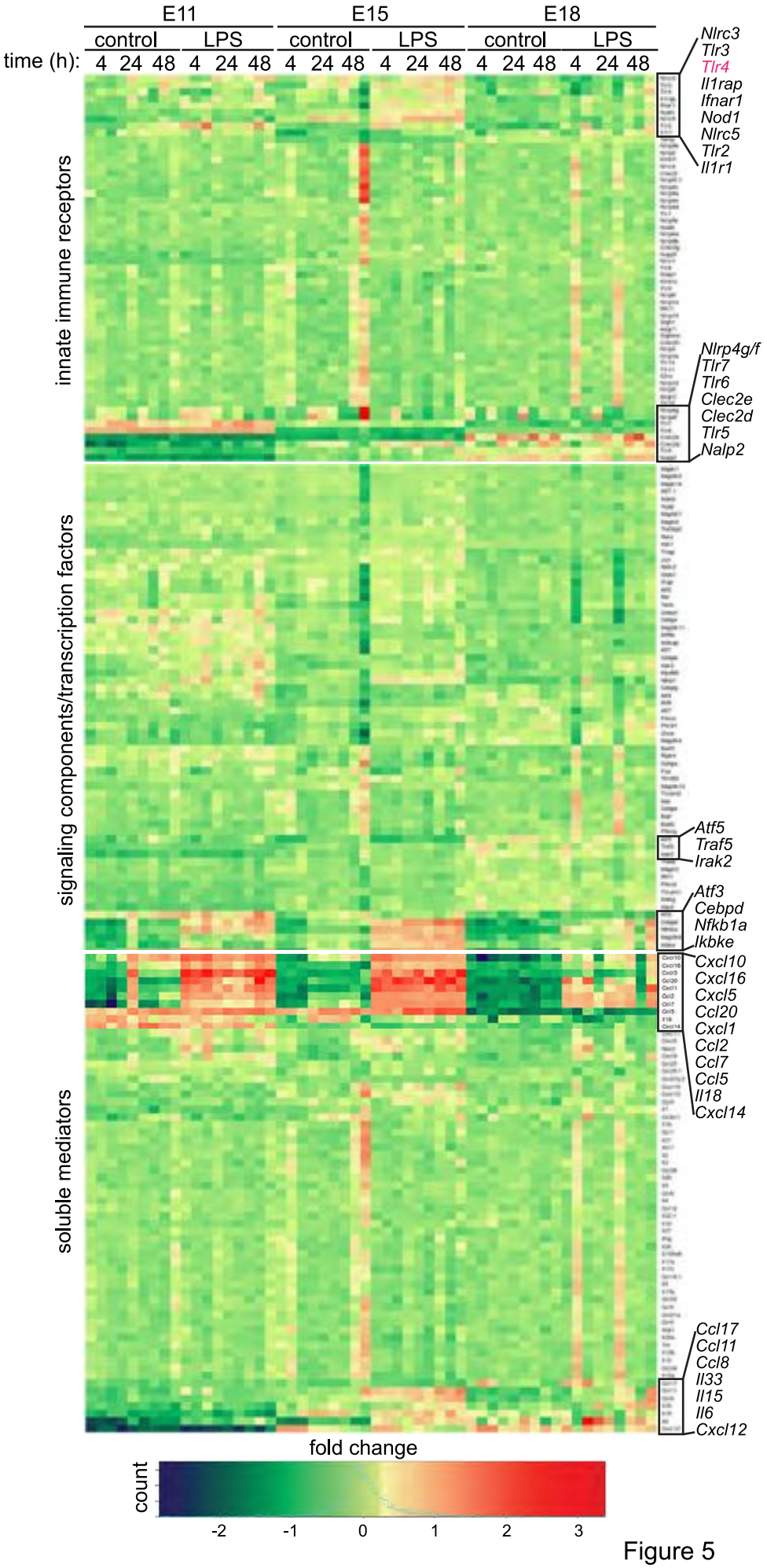
E11
E15
E18
control
LPS
time (h):
4 24 48
innate immune receptors
signaling components/transcription factors
soluble mediators
Nlrc3
Tlr3
Tlr4
Il1rap
Ifnar1
Nod1
Nlrc5
Tlr2
Il1r1
Nlrp4g/f
Tlr7
Tlr6
Clec2e
Clec2d
Tlr5
Nalp2
Atf5
Traf5
Irak2
Atf3
Cebpd
Nfkb1a
Ikbke
Cxcl10
Cxcl16
Cxcl5
Ccl20
Cxcl1
Ccl2
Ccl7
Ccl5
Il18
Cxcl14
Ccl17
Ccl11
Ccl8
Il33
Il15
Il6
Cxcl12
fold change
count
-2
-1
0
1
2
3

Figure 5

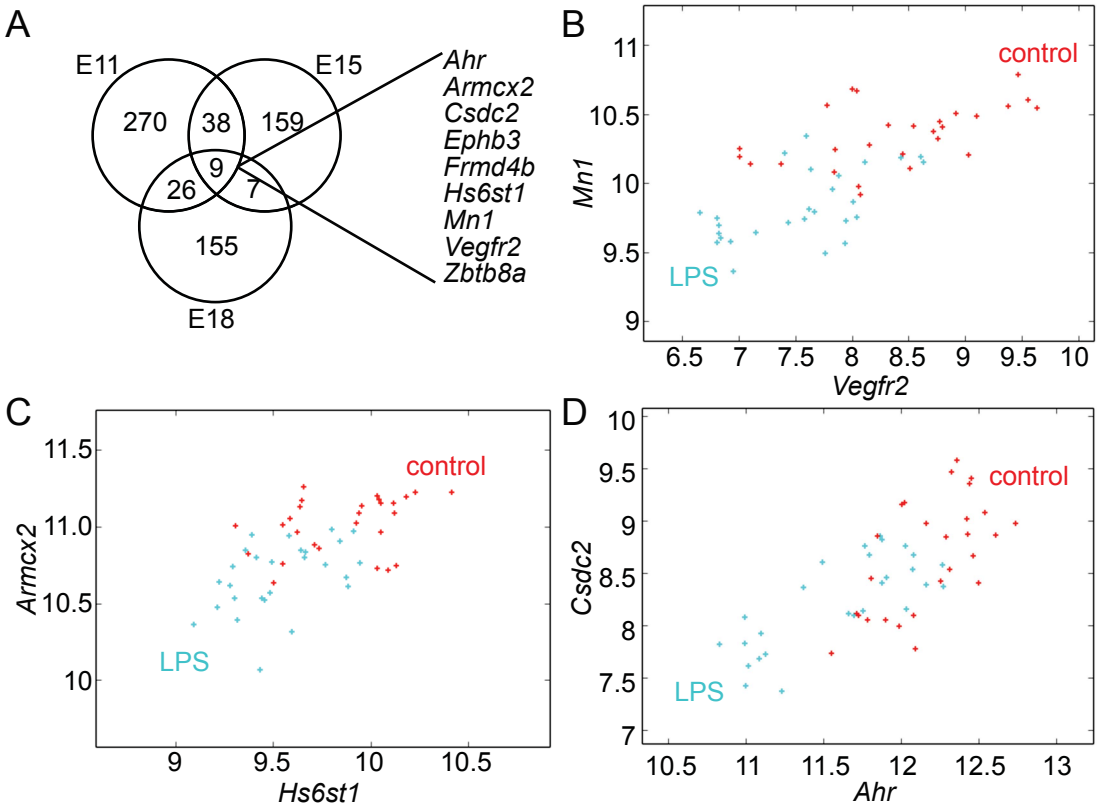
A
E11
E15
E18
270
38
159
9
26
7
155
Ahr
Armcx2
Csdc2
Ephb3
Frmd4b
Hs6st1
Mn1
Vegfr2
Zbtb8a
B
control
LPS
Mn1
Vegfr2
C
control
LPS
Armcx2
Hs6st1
D
control
LPS
Csdc2
Ahr

Figure 6

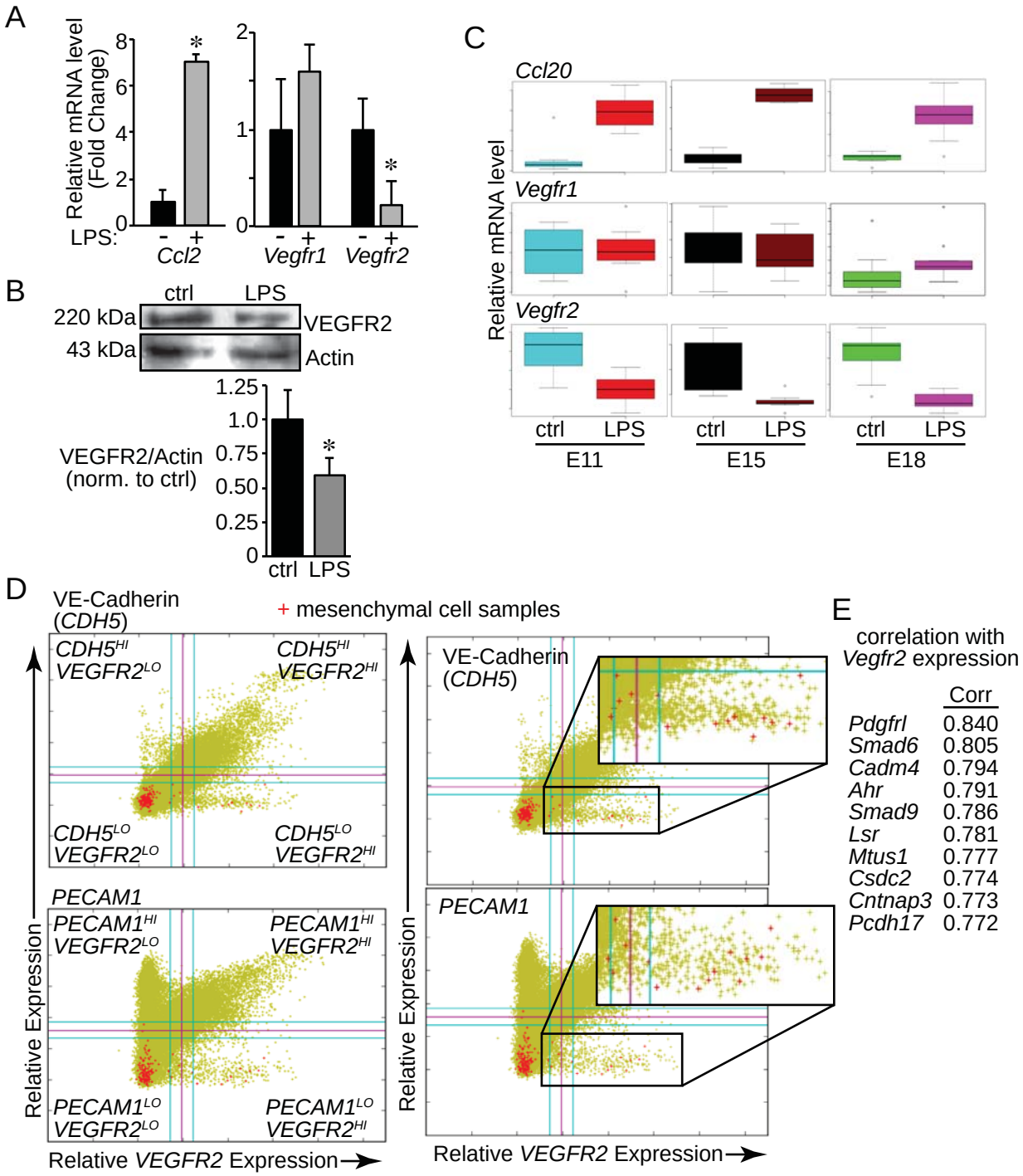
A
Relative mRNA level (Fold Change)
LPS:
Ccl2
Vegfr1
Vegfr2
B
ctrl
LPS
220 kDa
VEGFR2
43 kDa
Actin
VEGFR2/Actin (norm. to ctrl)
C
Ccl20
Vegfr1
Vegfr2
Relative mRNA level
E11
E15
E18
D
VE-Cadherin (CDH5)
+ mesenchymal cell samples
CDH5HI VEGFR2LO
CDH5HI VEGFR2HI
CDH5LO VEGFR2LO
CDH5LO VEGFR2HI
PECAM1
PECAM1HI VEGFR2LO
PECAM1HI VEGFR2HI
PECAM1LO VEGFR2LO
PECAM1LO VEGFR2HI
Relative Expression
Relative VEGFR2 Expression
E
correlation with Vegfr2 expression
Corr
Pdgfrl 0.840
Smad6 0.805
Cadm4 0.794
Ahr 0.791
Smad9 0.786
Lsr 0.781
Mtus1 0.777
Csdc2 0.774
Cntnap3 0.773
Pcdh17 0.772

Figure 7

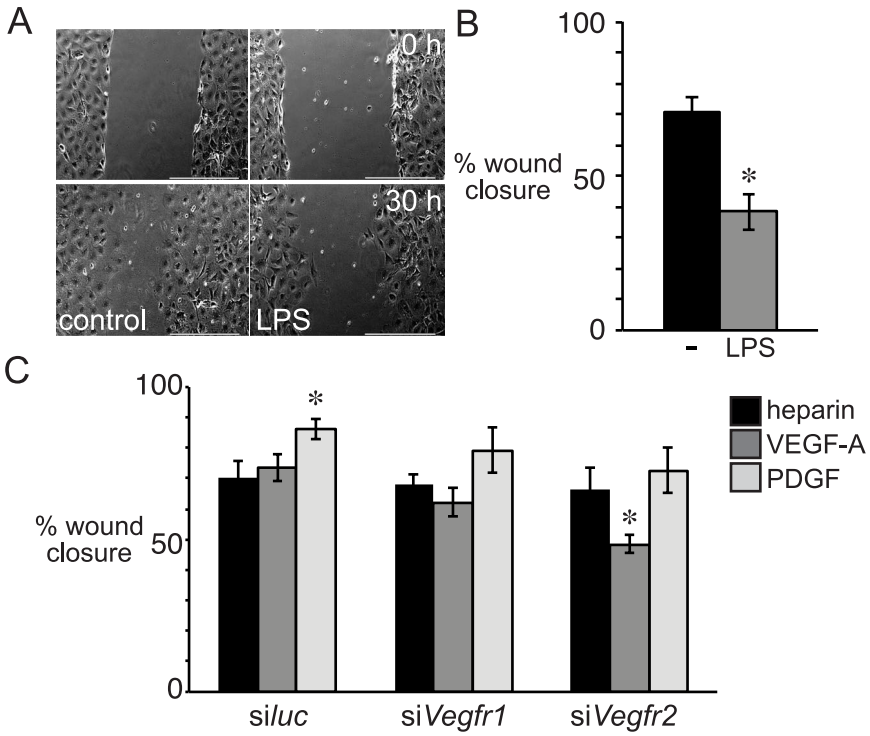
A
0 h
30 h
control
LPS
B
100
% wound closure
50
0
*
-
LPS
C
100
% wound closure
50
0
*
*
heparin
VEGF-A
PDGF
siluc
siVegfr1
siVegfr2

Figure 8

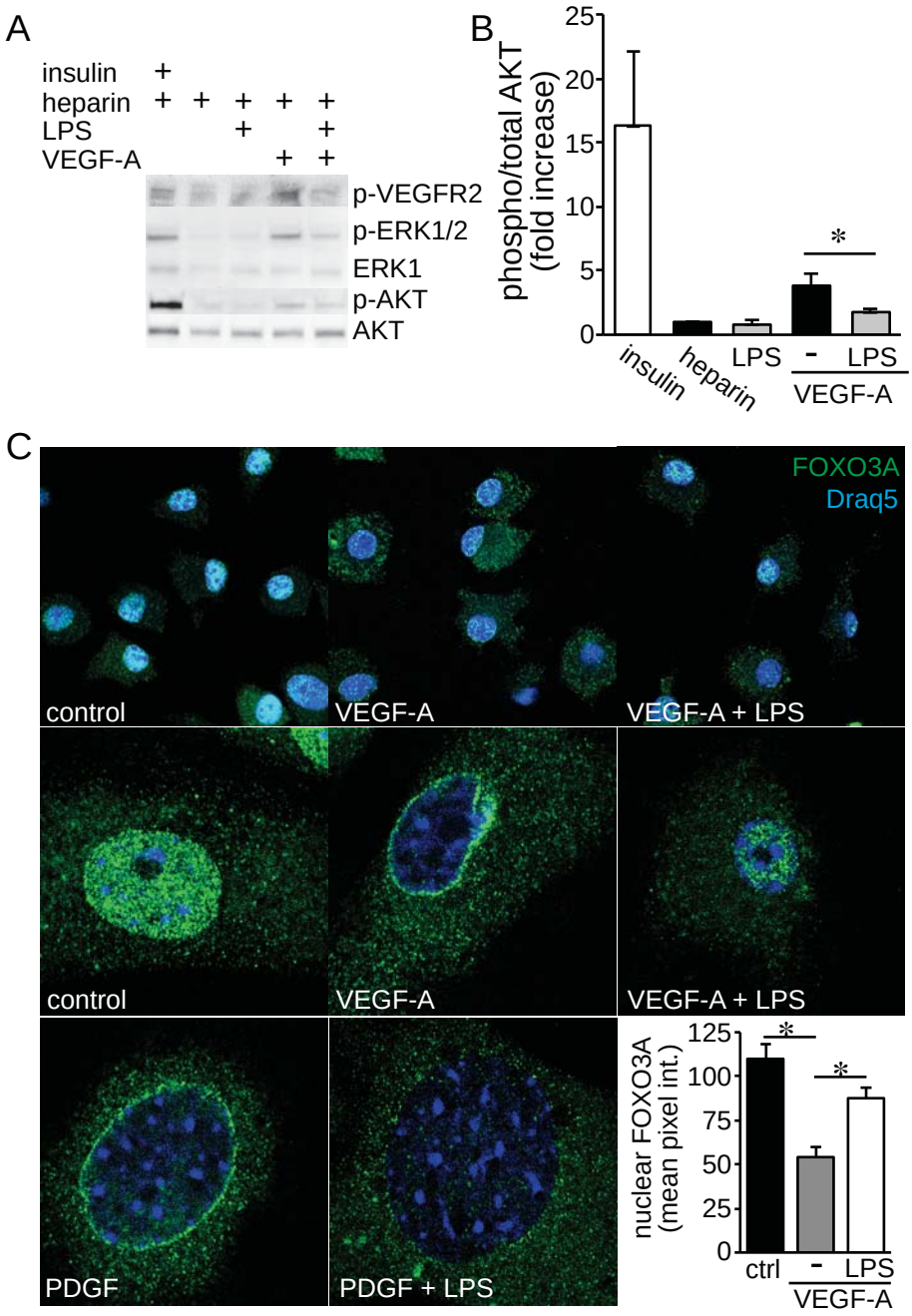
A
insulin +
heparin + + + + +
LPS + +
VEGF-A + +
p-VEGFR2
p-ERK1/2
ERK1
p-AKT
AKT
B
phospho/total AKT (fold increase)
25
20
15
10
5
0
*
insulin
heparin
LPS
-
LPS
VEGF-A
C
FOXO3A
Draq5
control
VEGF-A
VEGF-A + LPS
control
VEGF-A
VEGF-A + LPS
PDGF
PDGF + LPS
nuclear FOXO3A (mean pixel int.)
125
100
75
50
25
0
*
*
ctrl
-
LPS
VEGF-A

Figure 9

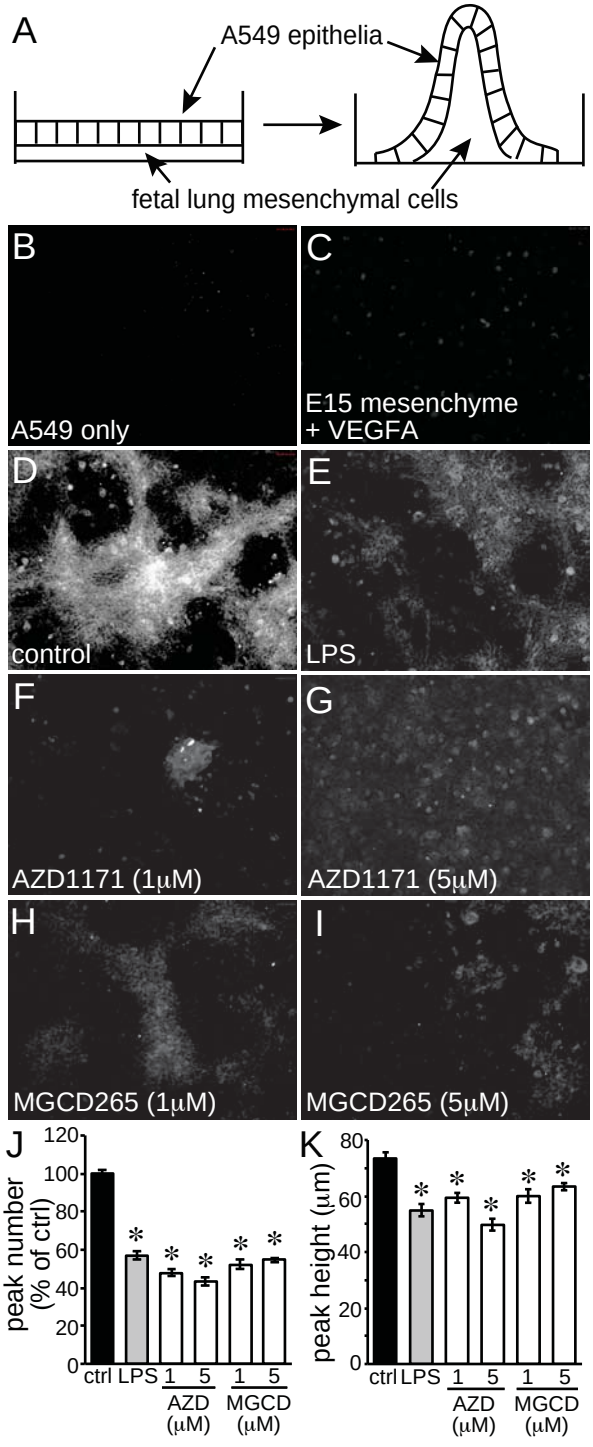
A
A549 epithelia
fetal lung mesenchymal cells
B
A549 only
C
E15 mesenchyme
+ VEGFA
D
control
E
LPS
F
AZD1171 (1μM)
G
AZD1171 (5μM)
H
MGCD265 (1μM)
I
MGCD265 (5μM)
J
peak number (% of ctrl)
120
100
80
60
40
20
0
ctrl LPS 1 5 1 5
AZD (μM)
MGCD (μM)
K
peak height (μm)
80
60
40
20
0
ctrl LPS 1 5 1 5
AZD (μM)
MGCD (μM)

Figure 10